JOURNAL OF GUIDANCE, CONTROL, AND DYNAMICS
Vol. 16, No. 1, January-February 1993

Optimal Control Law Synthesis for Flutter Suppression Using Active Acoustic Excitations

Pong-Jeu Lu* and Li-Jeng Huang†
National Cheng Kung University, Tainan, Taiwan 70101, Republic of China

This paper describes a development of the optimal control law design procedure for the flutter suppression of airfoils using active acoustic excitations. A bending-torsion typical section and a two-dimensional incompressible aerodynamic model are adopted for the present analysis. An irreducible state-space description of the aeroservoelastic system is constructed via the use of Hankel matrices and the singular value decomposition method. The evaluation of the degree of controllability/observability and the synthesis of the optimal control law using steady-state linear quadratic regulator theory accompanied by an asymptotic state observer are performed. This optimal control law design enables the search of the most effective position to locate the sound wave generator. The trailing edge is shown to be the best region for installing the sound wave generator, where the highest degree of controllability and the minimal control effort are attained. A case study shows that approximately 20 dB reduction in sound pressure level can be achieved using this optimal control law design.

Nomenclature

$\boldsymbol{A}$ = system matrix
a = location of elastic axis (nondimensionalized by b)
$\boldsymbol{B}$ = damping matrix
$\boldsymbol{b}$ = damping vector (when suffixed by subscript); also the input matrix
b = semichord length
$\boldsymbol{C}$ = controllability matrix
$\boldsymbol{c}$ = system output vector
d = output-to-input coefficient
$\boldsymbol{e}$ = state error vector
$\boldsymbol{f}$ = $\lfloor -bL, M_\alpha \rfloor^T$, generalized force vector
$\boldsymbol{g}$ = full-state controller gain vector
$\boldsymbol{g}_E$ = full-dimension observer gain vector
$H(\bar{s})$ = transfer function of the dynamic system
H_c = $\Phi_c/b^2\omega_\alpha$, nondimensional sound source strength
h = plunging displacement, positive downward
$\boldsymbol{I}$ = identity matrix
I_α = mass moment of inertia per unit span
J = cost functional (performance index)
$\boldsymbol{K}$ = stiffness matrix
K_h, K_α = spring constants for plunging and pitching modes, respectively
K_0, K_1 = modified Bessels functions of second kind of the zeroth and the first order, respectively
$\boldsymbol{k}$ = stiffness vector
L = lift per unit span
$\boldsymbol{M}$ = mass matrix
M_α = pitching moment per unit span about the elastic axis, positive nose up
m_s = mass per unit span of the typical section
n = number of states ($n = 6$)
$\boldsymbol{O}$ = observability matrix
Q = system state weighting coefficient
$\boldsymbol{q}$ = $\lfloor h/b, \alpha \rfloor^T$, generalized coordinate vector
R = control input weighting coefficient
r_c, θ_c = coordinates of sound source in Joukowski transform domain
r_α = $\sqrt{I_\alpha/m_s b^2}$, radius of gyration
S_α = static mass moment per unit span
$\bar{s}$ = s/ω_α, nondimensional Laplace transform variable
$\bar{t}$ = $\omega_\alpha t$, nondimensional time
$\bar{U}$ = $U/b\omega_\alpha$, nondimensional freestream speed
$\boldsymbol{u}$ = input vector
$\boldsymbol{x}, \boldsymbol{x}_0, \boldsymbol{x}_E$ = actual, initial, and estimated state vectors
x_c, z_c = nondimensional coordinates of sound source location
x_α = $S_\alpha/m_s b$, static unbalance
$\boldsymbol{y}$ = output vector
α = angle of incidence, positive nose up
η = $\rho b^2/m_s$, constant defined in Eq. (4b)
λ_i = singular values
μ_{co} = controllability/observability index
ρ = air density
Σ = diagonal matrix of singular values
σ = sb/U, nondimensional Laplace transform variable
Φ_c = volume flow rate or strength of the acoustic source
$\bar{\omega}$ = ω/ω_α, nondimensional circular frequency
ω_h, ω_α = uncoupled plunging and pitching natural frequencies, respectively

Superscripts

A = airfoil motion induced
C = acoustically induced
T = matrix transpose
$\bar{}$ = nondimensional variable
$\dot{}$ = time derivative
$\hat{}$ = quantity in the Laplace transform domain
-1 = matrix inverse

Subscripts

a = airfoil motion induced
ac = airfoil motion induced circulatory part
anc = airfoil motion induced noncirculatory part
c = acoustically induced
cc = acoustically induced circulatory part
cl = closed-loop
cnc = acoustically induced noncirculatory part
s = structural

Received Dec. 9, 1991; revision received April 27, 1992; accepted for publication May 29, 1992.

*Associate Professor, Institute of Aeronautics and Astronautics. Member AIAA.
†Graduate Research Assistant, Institute of Aeronautics and Astronautics.

I. Introduction

ACTIVE control technology (ACT) would be indispensable for many innovative designs associated with future energy-efficient transports and control-configured vehicles. Active flutter suppression (AFS) belongs to one of these ACT concepts, for which the aim is to increase the critical flutter boundary under a given structural condition. In past decades, extensive research has been carried out toward developing active flutter suppression and gust alleviation techniques.[1-9] The hydraulically actuated aerodynamic control surfaces, such as the trailing-edge and leading-edge flaps, have been employed as the aeroelastic control actuators. However, fundamental difficulties exist in the implementation of such ACTs using the mechanically driven control surfaces. One of the major problems lies in the intrinsic characteristic of the servomechanism, namely, the hydraulic actuator is usually sluggish in response so that it cannot cope with high-frequency oscillations.

Recently, an innovative flutter control technique based on the *antisound* concept[10,11] was successfully demonstrated.[12] In this pioneering experimental work, a sound wave was used to suppress the fluttering airfoil motion. The implication and impact to the AFS technique is revolutionary, since the difficulties encountered in the aforementioned servomechanism can be completely circumvented. The electronically actuated acoustic device not only can reduce the weight required but also can provide a wide range of frequency bandwidth for which the actuator response can almost be instantaneous. To explain the underlying acoustic flutter suppression mechanism, Lu and Huang[13] have conducted a theoretical investigation that shows that it is the *trailing edge receptivity*, rather than the hydraulic analogy originally proposed,[12] that plays the dominant role in suppressing the flutter instabilities. In other words, the control force is not the sound itself but is the acoustically induced shedding vorticities that form the basic flutter suppression mechanism. Among those important parameters, the phase angle between the acoustic excitation and the sensed airfoil motions primarily determines the stability of the closed-loop aeroelastic system, whereas the magnitude of the sound strength affects the damping rate of the suppressed transient responses.

To further explore this new flutter suppression technique, an optimization of the feedback control law is necessary. The minimized sound pressure level may lead to a low-energy, lightweight miniaturization of the acoustic wave generator. This will be of particular significance for the practical implementation of the present new AFS technique. In Ref. 13, a preliminary control strategy was proposed using the output feedback control laws. In order to investigate system controllability and observability and to perform the optimal control laws synthesis, a state-space analysis is employed presently. The active acoustic flutter control technique can, therefore, be elucidated in detail, providing a basic design groundwork for the future practical realization of this newly discovered technique.

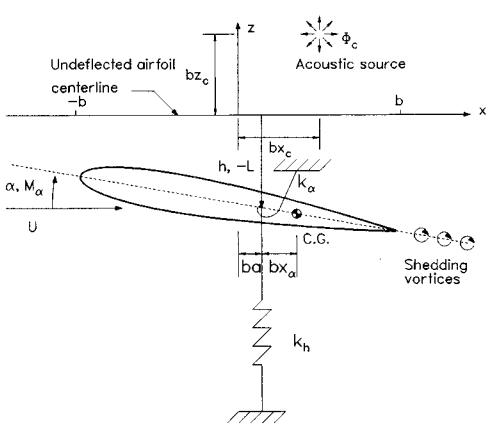

Fig. 1 Schematic of a typical section model with acoustic excitation (internal excitation $z_c = 0^+$ for the present case).

This paper presents a state-space optimal flutter control law analysis for thin airfoils using an active acoustic excitation technique. Closed-form unsteady, incompressible aerodynamic loads induced by a harmonically excited acoustic monopole derived in Ref. 13 are used. The Padé approximant[1-5] is employed to represent the transcendental-type generalized Theodorsen's function, which makes the present infinite dimensional aeroservoelastic system be reduced into a finite dimensional one. An irreducible state-space description (SSD) is then obtained from the polynomial matrix description (PMD) of the dynamic system via the Hankel matrix and the singular value decomposition method. The degree of controllability/observability of the aeroservoelastic system as a function of the acoustic excitation position is examined. The results basically agree with those obtained using the steady-state linear quadratic regulator (SSLQR) theory. Because of the fact that the states are often not measurable using the present state-space realization method, an observer design is also proposed. It is demonstrated that the use of the concept of trailing-edge receptivity in conjunction with optimal control theory may lead to a substantial reduction of the control effort that is required.

II. Aeroservoelastic System Model

The aeroservoelastic model used for the present study is depicted in Fig. 1. It consists of a bending-torsion typical wing section and an internal acoustic wave generator. The sound waves, generated by any acoustic devices, are emitted into the airstream from the airfoil surface. The equations of motion for this two-dimensional dynamic system can be written as

$$\boldsymbol{M}_s\ddot{\boldsymbol{q}} + \omega_\alpha^2 \boldsymbol{K}_s \boldsymbol{q} = \frac{1}{m_s b^2}\{\boldsymbol{f}^A + \boldsymbol{f}^C\} \tag{1}$$

in which the structural mass and stiffness matrices $\boldsymbol{M}_s$ and $\boldsymbol{K}_s$ are defined as follows:

$$\boldsymbol{M}_s = \begin{bmatrix} 1 & x_\alpha \\ x_\alpha & r_\alpha^2 \end{bmatrix}, \qquad \boldsymbol{K}_s = \begin{bmatrix} (\omega_h/\omega_\alpha)^2 & 0 \\ 0 & r_\alpha^2 \end{bmatrix}$$

The aerodynamic load vector $\boldsymbol{f}^A$ induced by harmonic airfoil motions in a two-dimensional incompressible flow has been derived by Theodorsen.[14] These formulas were later extended by Sears[15] to arbitrary motions, which take the following form in the Laplace transform domain:

$$\hat{\boldsymbol{f}}^A = \rho b^4 \omega_\alpha^2 \left[\bar{s}^2 \boldsymbol{M}_{anc} + \bar{s}\bar{U}\boldsymbol{B}_{anc} + \bar{U}^2 \boldsymbol{K}_{anc} + (\bar{s}\bar{U}\boldsymbol{B}_{ac} + \bar{U}^2 \boldsymbol{K}_{ac}) C(\sigma)\right] \hat{\boldsymbol{q}} \tag{2}$$

where the constant matrices $\boldsymbol{M}_{anc}$, $\boldsymbol{B}_{anc}$, $\boldsymbol{K}_{anc}$, $\boldsymbol{B}_{ac}$, and $\boldsymbol{K}_{ac}$ are given below:

$$\boldsymbol{M}_{anc} = \begin{bmatrix} -\pi & \pi a \\ \pi a & -\pi(\tfrac{1}{8} + a^2) \end{bmatrix}$$

$$\boldsymbol{B}_{anc} = \begin{bmatrix} 0 & -\pi \\ 0 & -\pi(\tfrac{1}{2} - a) \end{bmatrix}, \qquad \boldsymbol{K}_{anc} = \begin{bmatrix} 0 & 0 \\ 0 & 0 \end{bmatrix}$$

$$\boldsymbol{B}_{ac} = \begin{bmatrix} -2\pi & -2\pi(\tfrac{1}{2} - a) \\ 2\pi(\tfrac{1}{2} + a) & 2\pi(\tfrac{1}{2} + a)(\tfrac{1}{2} - a) \end{bmatrix}$$

$$\boldsymbol{K}_{ac} = \begin{bmatrix} 0 & -2\pi \\ 0 & 2\pi(\tfrac{1}{2} + a) \end{bmatrix}$$

In Eq. (2), the function $C(\sigma)$ represents the generalized Theodorsen's function and is given by

$$C(\sigma) = \frac{K_1(\sigma)}{K_1(\sigma) + K_0(\sigma)}$$

The aerodynamic load vector $\boldsymbol{f}^C$ induced by the acoustic excitation, however, has recently been derived by the authors in the Laplace transform domain as[13]

$$\hat{\boldsymbol{f}}^C = \rho b^4 \omega_\alpha^2 \left\{\bar{s}\boldsymbol{b}_{cnc} + \bar{U}\boldsymbol{k}_{cnc} + \bar{U}\boldsymbol{k}_{cc} C(\sigma)\right\} \hat{H}_c \tag{3}$$

in which the constant matrices $\boldsymbol{b}_{cnc}$, $\boldsymbol{k}_{cnc}$, and $\boldsymbol{k}_{cc}$ are defined, respectively, as

$$\boldsymbol{b}_{cnc} = \begin{bmatrix} -E_1 \\ E_3 + aE_1 \end{bmatrix}, \qquad \boldsymbol{k}_{cnc} = \begin{bmatrix} 0 \\ E_4 - \pi E_5 \end{bmatrix}$$

$$\boldsymbol{k}_{cc} = \begin{bmatrix} -2\pi E_5 \\ 2\pi(\tfrac{1}{2} + a)E_5 \end{bmatrix}$$

The variables E_1, E_2, E_3, E_4, and E_5 appearing in these entries are defined as

$$E_1 = -\frac{\sin\theta_c}{r_c}, \qquad E_2 = 0, \qquad E_3 = \frac{1}{2}\frac{\sin\theta_c \cos\theta_c}{r_c^2}$$

$$E_4 = -\frac{\sin\theta_c}{r_c}, \qquad E_5 = \frac{-1}{\pi}\frac{r_c \sin\theta_c}{1 + r_c^2 - 2r_c\cos\theta_c}$$

Upon substituting Eqs. (2) and (3) into Eq. (1), the equations of motion of the oscillating typical section forced by an acoustic wave generator can be expressed in the Laplace transform domain as

$$\left[\bar{s}^2\boldsymbol{A}_2 + \bar{s}\boldsymbol{A}_1 + \boldsymbol{A}_0 + (\bar{s}\boldsymbol{B}_1 + \boldsymbol{B}_0)C(\sigma)\right]\hat{\boldsymbol{q}} = \left[\bar{s}\boldsymbol{C}_1 + \boldsymbol{C}_0 + \boldsymbol{D}_0 C(\sigma)\right]\hat{H}_c \tag{4a}$$

with the coefficient matrices given by

$$\boldsymbol{A}_2 = \boldsymbol{M}_s - \eta\boldsymbol{M}_{anc}, \quad \boldsymbol{A}_1 = -\eta\bar{U}\boldsymbol{B}_{anc}, \quad \boldsymbol{A}_0 = \boldsymbol{K}_s - \eta\bar{U}^2\boldsymbol{K}_{anc}$$

$$\boldsymbol{B}_1 = -\eta\bar{U}\boldsymbol{B}_{ac}, \qquad \boldsymbol{B}_0 = -\eta\bar{U}^2\boldsymbol{K}_{ac}$$

$$\boldsymbol{C}_1 = \eta\boldsymbol{b}_{cnc}, \qquad \boldsymbol{C}_0 = \eta\bar{U}\boldsymbol{k}_{cnc}, \qquad \boldsymbol{D}_0 = \eta\bar{U}\boldsymbol{k}_{cc} \tag{4b}$$

III. State Space Realization

In order to obtain an expression that is suitable for the finite dimensional aeroservoelastic analysis, we use the R. T. Jones approximation (or a second-order Padé approximant) of the generalized Theodorsen's function[16]

$$C(\sigma) \approx \frac{0.5\sigma^2 + 0.2808\sigma + 0.01365}{\sigma^2 + 0.3455\sigma + 0.01365} \tag{5}$$

The accuracy of this approximation has been evaluated and discussed.[17,18] Substituting Eq. (5) into Eq. (4a) and then multiplying Eq. (4a) by the denominator of Eq. (5), we can obtain

$$(\bar{s}^4\boldsymbol{P}_4 + \bar{s}^3\boldsymbol{P}_3 + \bar{s}^2\boldsymbol{P}_2 + \bar{s}^1\boldsymbol{P}_1 + \boldsymbol{P}_0)\hat{\boldsymbol{q}} = (\bar{s}^3\boldsymbol{Q}_3 + \bar{s}^2\boldsymbol{Q}_2 + \bar{s}^1\boldsymbol{Q}_1 + \boldsymbol{Q}_0)\hat{H}_c \tag{6}$$

where

$$\boldsymbol{P}_4 = \boldsymbol{A}_2$$

$$\boldsymbol{P}_3 = \boldsymbol{A}_1 + 0.3455\bar{U}\boldsymbol{A}_2 + 0.5\boldsymbol{B}_1$$

$$\boldsymbol{P}_2 = \boldsymbol{A}_0 + 0.3455\bar{U}\boldsymbol{A}_1 + 0.01365\bar{U}^2\boldsymbol{A}_2 + 0.5\boldsymbol{B}_0 + 0.2808\bar{U}\boldsymbol{B}_1$$

$$\boldsymbol{P}_1 = 0.3455\bar{U}\boldsymbol{A}_0 + 0.01365\bar{U}^2\boldsymbol{A}_1 + 0.2808\bar{U}\boldsymbol{B}_0 + 0.01365\bar{U}^2\boldsymbol{B}_1$$

$$\boldsymbol{P}_0 = 0.01365\bar{U}^2\boldsymbol{A}_0 + 0.01365\bar{U}^2\boldsymbol{B}_0$$

$$\boldsymbol{Q}_3 = \boldsymbol{C}_1 + 0.5\boldsymbol{D}_1$$

$$\boldsymbol{Q}_2 = \boldsymbol{C}_0 + 0.3455\bar{U}\boldsymbol{C}_1 + 0.5\boldsymbol{D}_0 + 0.2808\bar{U}\boldsymbol{D}_1$$

$$\boldsymbol{Q}_1 = 0.3455\bar{U}\boldsymbol{C}_0 + 0.01365\bar{U}^2\boldsymbol{C}_1 + 0.2808\bar{U}\boldsymbol{D}_0 + 0.01365\bar{U}^2\boldsymbol{D}_1$$

$$\boldsymbol{Q}_0 = 0.01365\bar{U}^2\boldsymbol{C}_0 + 0.01365\bar{U}^2\boldsymbol{D}_0$$

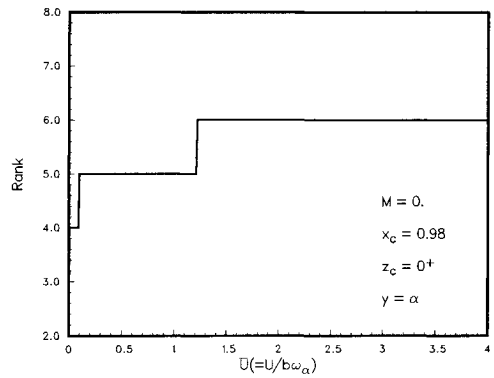

Fig. 2 Rank of the state-space model vs the nondimensional flight speed $U/b\omega_\alpha$.

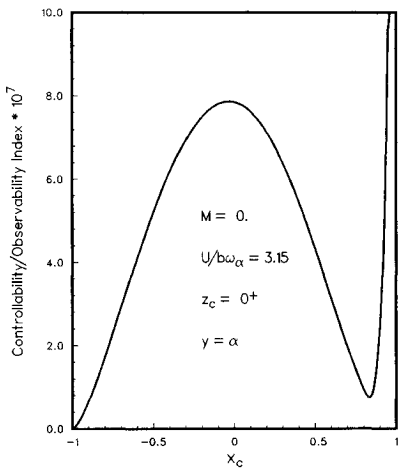

Fig. 3 Controllability/observability index vs the acoustic excitation position ($y = \alpha$).

We now arrive at a PMD of the dynamic system, which can be abbreviated as

$$\boldsymbol{P}(\bar{s})\hat{\boldsymbol{q}} = \boldsymbol{Q}(\bar{s})\hat{H}_c \tag{7}$$

Note that $\boldsymbol{P}(\bar{s})$ and $\boldsymbol{Q}(\bar{s})$ are the matrix polynomial functions whose parameters include the flight speed and the acoustic excitation position, provided that the structural properties are given fixed.

It is important to remark here that the existence of the high-order polynomials on the right-hand side and the absence of the servo-actuator dynamics make Eq. (7) difficult to be converted into a jointly controllable and observable system simply by direct speculation, such as in the conventional flutter control synthesis using the control surfaces.[1,4] To avoid the drawback of introducing high-order derivatives ($\dot{H}_c$, $\ddot{H}_c, \ldots$, etc.) in the system input vector,[2,5] an alternative that can directly lead to a jointly controllable and observable system is developed for the present acoustic flutter supression investigation.

An internally balanced realization of a minimal-dimensional state-space description of the dynamic system can be constructed via the Hankel matrix and the singular value decomposition method,[19] as described briefly as follows. First, we can select a measurable output variable to be the plunging deformation h/b, the pitching deformation α, or any other conveniently defined variable; then relate this output variable to the generalized coordinates by the formula

$$\hat{y} = \left[\boldsymbol{r}_0 + \bar{s}\boldsymbol{r}_1 + \bar{s}^2\boldsymbol{r}_2\right]\hat{\boldsymbol{q}} = \boldsymbol{r}(\bar{s})\hat{\boldsymbol{q}} \tag{8}$$

where $\boldsymbol{r}_0$, $\boldsymbol{r}_1$, and $\boldsymbol{r}_2$ are the appropriately defined row vectors.

Thus, the transfer function connecting the output and the input variables can be established:

$$H(\bar{s}) = \frac{\hat{y}(\bar{s})}{\hat{H}_c(\bar{s})} = \boldsymbol{r}(\bar{s})\boldsymbol{P}^{-1}(\bar{s})\boldsymbol{Q}(\bar{s}) \tag{9}$$

For the present problem, $\boldsymbol{P}$ is a 2×2 matrix polynomial of fourth order in $\bar{s}$ and, thus, the denominator of the transfer function is an eighth-order polynomial function of $\bar{s}$ and $\bar{U}$.

The transfer function $H(\bar{s})$ can be expanded into an infinite power series in descending order of $\bar{s}$ like

$$H(\bar{s}) = H(0) + H(1)\bar{s}^{-1} + H(2)\bar{s}^{-2} + \cdots \tag{10}$$

where $H(0), H(1), \ldots$ are termed the Markov parameters, with which one can define the following two 8×8 Hankel matrices:

$$\boldsymbol{T} = \begin{bmatrix} H(1) & H(2) & \cdots & H(8) \\ H(2) & H(3) & \cdots & H(9) \\ \vdots & \vdots & & \vdots \\ H(8) & H(9) & \cdots & H(15) \end{bmatrix} \tag{11a}$$

$$\boldsymbol{T}^+ = \begin{bmatrix} H(2) & H(3) & \cdots & H(9) \\ H(3) & H(4) & \cdots & H(10) \\ \vdots & \vdots & & \vdots \\ H(9) & H(10) & \cdots & H(16) \end{bmatrix} \tag{11b}$$

Then the matrix $\boldsymbol{T}$ can be decomposed, using the singular value decomposition method, into

$$\boldsymbol{T} = \boldsymbol{K}\begin{bmatrix} \Sigma & 0 \\ 0 & 0 \end{bmatrix}\boldsymbol{L} \tag{12}$$

where the diagonal matrix $\Sigma = \text{diag}\{\lambda_1, \lambda_2, \ldots, \lambda_n\}$ is composed of λ_i, $i = 1, 2, \ldots, n$, the positive singular values. Notice that n is the rank of the matrix $\boldsymbol{T}$ and is the minimal dimension of the irreducibly realized system. Letting $\boldsymbol{K}_1$ denote the first n columns of $\boldsymbol{K}$ and $\boldsymbol{L}_1$ be the first n rows of $\boldsymbol{L}$, one can write $\boldsymbol{T}$ alternatively as

$$\boldsymbol{T} = \boldsymbol{K}_1\Sigma\boldsymbol{L}_1 = \boldsymbol{K}_1\Sigma^{1/2}\Sigma^{1/2}\boldsymbol{L}_1 = \boldsymbol{V}\boldsymbol{U} \tag{13}$$

where

$$\Sigma^{1/2} = \text{diag}\{\sqrt{\lambda_1}, \sqrt{\lambda_2}, \ldots, \sqrt{\lambda_n}\}$$

$\boldsymbol{V} = \boldsymbol{K}_1\Sigma^{1/2}$, and $\boldsymbol{U} = \Sigma^{1/2}\boldsymbol{L}_1$. By further defining

$$\boldsymbol{V}^+ = \Sigma^{-1/2}\boldsymbol{K}_1^T \quad \text{and} \quad \boldsymbol{U}^+ = \boldsymbol{L}_1^T\Sigma^{-1/2} \tag{14}$$

the irreducible realization of $H(\bar{s})$ is found to be

$$\frac{d\boldsymbol{x}}{d\bar{t}} = \boldsymbol{A}\boldsymbol{x} + \boldsymbol{b}u \tag{15a}$$

$$y = \boldsymbol{c}\boldsymbol{x} + du \tag{15b}$$

where

$$\boldsymbol{A} = \boldsymbol{V}^+\boldsymbol{T}^+\boldsymbol{U}^+$$

$\boldsymbol{b}$ = the first column of $\boldsymbol{U}$

$\boldsymbol{c}$ = the first row of $\boldsymbol{V}$

$$d = H(0) \tag{15c}$$

In Eqs. (15), $\boldsymbol{x}$ is a state vector consisting of the linear combinations of the structural states, the rates of change of these states, and the aerodynamic lag terms as well. The control variable u (a scalar representing the nondimensional acoustic strength $\hat{H}_c$ for the present case) remains unchanged, which would not be so if other existing realization methods were used.

A typical example with parameters listed in Table 1 was selected for numerically studying the state-space realization just proposed. The flight speed is selected to be $\bar{U} = 3.15$, approximately 5% higher than the open-loop flutter speed, and the output variable is the pitching displacement $y = \alpha$. The resulting system matrices $\boldsymbol{A}$, $\boldsymbol{b}$, and $\boldsymbol{c}$ for the realized dynamic system are listed in Table 1. The minimal dimension of this open-loop aeroelastic system is six, which agrees with that obtained using the minimum-state realization method.[1,4] After a careful examination of the system matrices listed in Table 1, it can be found that the realization achieved is inherently balanced.

It is noteworthy that the rank of the Hankel matrices (and, thus, the minimal dimension of the realized dynamic system) depends on the selected freestream speed and the output variable. This is because the coefficient matrices $\boldsymbol{P}(\bar{s})$ and $\boldsymbol{Q}(\bar{s})$ in the PMD are functions of the flight speed $\bar{U}$ and because the Markov parameters $H(0), H(1), \ldots$ are obtained from the transfer function representing the input-output relationship.

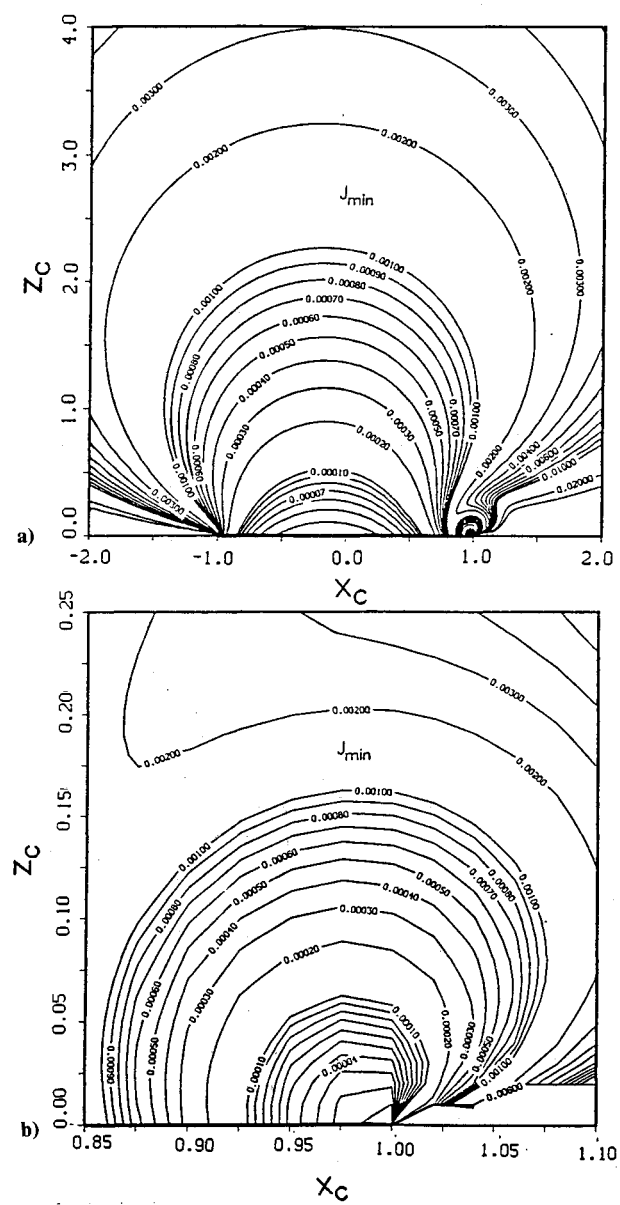

Fig. 4 Control cost contours: a) global view and b) blowup view in the vicinity of the trailing edge.

Table 1 Minimal-dimensional SSD of the 2-DOF typical section model with an acoustic excitation ($x_\alpha = 0.2$, $r_\alpha = 0.5$, $\omega_h = 50$ rad/s, $\omega_\alpha = 100$ rad/s, $a = -0.4$, $\mu = 40$, $x_c = 0.98$, $z_c = 0^+$, $y = \alpha$, $\bar{U} = 3.15$)

$$A = \begin{bmatrix} -0.4445 & 0.7251 & 0.0957 & 0.0501 & -0.0486 & 0.0006 \\ -0.7251 & 0.0414 & -0.1595 & -0.0891 & 0.0777 & -0.0012 \\ 0.0957 & 0.1595 & -0.7972 & 0.1704 & -0.2265 & 0.0059 \\ -0.0501 & -0.0891 & -0.1704 & -0.2685 & -0.7900 & -0.0144 \\ -0.0486 & -0.0771 & -0.2265 & 0.7900 & 0.2604 & -0.0130 \\ 0.0006 & 0.0012 & 0.0059 & 0.0144 & -0.0130 & -0.1345 \end{bmatrix}$$

$$b^T = [-0.4421 \quad 0.4524 \quad 0.0647 \quad -0.0439 \quad -0.0436 \quad 0.0008]$$

$$c = [0.4421 \quad 0.4524 \quad -0.0647 \quad -0.0439 \quad 0.0436 \quad -0.0008]$$

The rank of the Hankel matrices vs the freestream speed for the present representative system is shown in Fig. 2. It is seen that the dimension of the realized system is initially four, as expected, for the typical section in the free vibration limit ($\bar{U} = 0$), since only four states exist corresponding to the structural modes and they involve no aerodynamic lag modes. As the freestream speed increases, the influence of the aerodynamic lag modes comes in and becomes more influential, and the resulting rank of the Hankel matrices increases, starting from five, where the aerodynamic lag mode $\bar{s} = -0.3\bar{U}$ is included, to six, where both the aerodynamic lag modes $\bar{s} = -0.3\bar{U}$ and $\bar{s} = -0.0455\bar{U}$ are contained.

It would be of interest to see whether the present SSD of the realized system possesses closely enough the dynamic behavior described by the original PMD before it can be used for the optimal control law synthesis. First of all, the open-loop poles obtained from the SSD should coincide with the poles of the transfer function associated with the PMD. From Eqs. (15a) and (15b) it can be seen that the roots of the characteristic equation of the SSD are the poles of the transfer function:

$$H(\bar{s}) = c(\bar{s}I - A)^{-1}b + d \tag{16}$$

These eigenvalues are listed in Table 2. Also listed in Table 2 are the roots obtained from the PMD of the system. The agreement is seen to be excellent for these two descriptions. Moreover, the nonphysical poles corresponding to the two aerodynamic lag modes appearing in the PMD are automatically canceled by the zeros of the numerator in the SSD realization. In other words, the present irreducible realization avoids the drawback of introducing nonphysical augmented states in the aeroservoelastic system formulation. Moreover, a reduced-order system can be obtained by a systematic way of deleting relatively unimportant singular values. This property is especially valuable since reduction in computational effort will be substantial, as the dimension of the full-state aeroservoelastic system is large and the number of aerodynamic lag terms cannot be lowered for accurate unsteady aerodynamic modeling.

Table 2 Comparison of eigenvalues obtained using PMD and SSD of the dynamic system

	Poles of the transfer function, PMD	Eigenvalues of the dynamic system, SSD
1	-0.7768[a]	-0.7768[a]
2	-0.9450[a]	
3	-0.1337[a]	-0.1337[a]
4	-0.1433[a]	
5	$0.0433 + 0.7089i$	$0.0433 + 0.7089i$
6	$0.0433 - 0.7089i$	$0.0433 - 0.7089i$
7	$-0.2595 + 0.7232i$	$-0.2595 + 0.7232i$
8	$-0.2595 - 0.7232i$	$-0.2595 - 0.7232i$

[a]Aerodynamic lag modes.

IV. Degree of Controllability and Observability

It is well known that a minimal realization can yield a jointly controllable and observable dynamic system. Many well-established approaches, such as the Kalman rank test, Popov-Belevitch-Hautus (PBH) rank test, and Davison eigenvalue test, etc.,[20] can be employed to check the joint controllability and observability of the system. For the present problem, the degree of controllability/observability of the dynamic system is of particular significance for determining the position at which the control input (acoustic waves generator) will be most effective. Among many approaches,[21-24] the one that uses the determinant of the inverse of the controllability/observability matrix[19] is employed. Following this line, we may define the controllability/observability index as

$$\mu_{co} = \det(C^{-1}) = \det(O^{-1}) \tag{17}$$

where C is the controllability matrix:

$$C = [b, Ab, \ldots, A^{n-1}b]$$

and O is the observability matrix:

$$O = \begin{bmatrix} c \\ cA \\ \vdots \\ cA^{n-1} \end{bmatrix}$$

The variation in degree of controllability/observability as a function of the acoustic excitation position moving along the airfoil surface is shown in Fig. 3. It is observed that regions near the airfoil midchord and trailing edge are the two "good" regions where the local or the absolute maximal controllability and observability occurs. Based on this observation, the control input (acoustic wave generator) and the sensor measuring the output signal can be suggested to be located in the vicinity of the trailing edge or the midchord of the airfoil.

V. Optimal Control Law Synthesis

To investigate flutter suppression by the use of an optimized acoustic control force, SSLQR theory is employed. Thus, a control logic is sought to minimize a quadratic objective function, consisting of the system output y and the control input u:

$$J_{\min} = \frac{1}{2}\int_0^\infty (Qy^2 + Ru^2)\, d\bar{t} \tag{18}$$

while subject to the equations of motion, Eq. (15). The solution to this optimal SSLQR problem is a linear, full-state, time-invariant feedback control law:

$$u = gx = -R^{-1}b^T Px \tag{19}$$

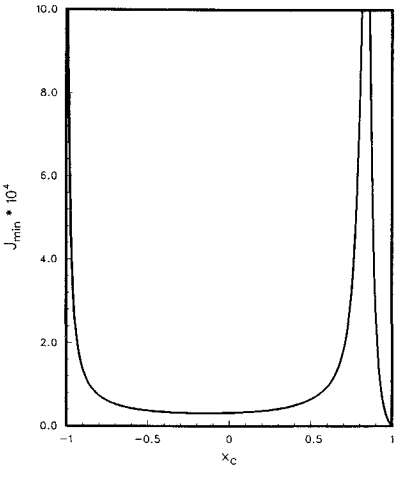

Fig. 5 Control cost function along the airfoil upper surface.

where $\boldsymbol{P}$ is the solution to the algebraic matrix Riccati equation

$$\boldsymbol{PA} + \boldsymbol{A}^T\boldsymbol{P} - \boldsymbol{PbR}^{-1}\boldsymbol{b}^T\boldsymbol{P} + \boldsymbol{c}^T\boldsymbol{Qc} = 0 \tag{20}$$

There are many algorithms that can be used to numerically solve this algebraic matrix Riccati equation.[20,25] For the present investigation, the MacFarlane-Potter-Fath method[20] is employed. The minimal cost function can be found in relation to $\boldsymbol{P}$ as

$$J_{\min} = \tfrac{1}{2}\boldsymbol{x}_0\boldsymbol{P}\boldsymbol{x}_0 \tag{21}$$

where $\boldsymbol{x}_0$ stands for the initial condition of the state vector. The closed-loop dynamic system then becomes

$$\frac{\mathrm{d}\boldsymbol{x}}{\mathrm{d}\bar{t}} = (\boldsymbol{A} + \boldsymbol{bg})\boldsymbol{x} = (\boldsymbol{A} + \boldsymbol{bR}^{-1}\boldsymbol{b}^T\boldsymbol{P})\boldsymbol{x} \tag{22}$$

The performance of the closed-loop system depends on the selection of the weighting coefficients Q and R. It is understood that the larger Q implies that more emphasis is placed on returning the system states to the origin (the equilibrium condition). On the other hand, raising R emphasizes the intention of reducing the amount of the control effort. A special result of the SSLQR theory is the case where $Q=0$ (i.e., zero-state weighting). For such an arrangement, the action of the resulting optimal control law upon the closed-loop eigenvalues is to leave unchanged all stable eigenvalues, while relocating the open-loop unstable eigenvalues originally located at $\bar{s}=\bar{s}_R+i\bar{\omega}$ to the stabilized mirror-image $\bar{s}=-\bar{s}_R+i\bar{\omega}$ about the imaginary axis.[20] This provides an attractive design method in constructing a desired stable closed-loop system.

Recall that for an infinite final-time SSLQR problem the system should be completely controllable in order to assure that the minimum cost is finite. The present irreducible SSD realization of the aeroelastic model yields a jointly controllable and observable system, guaranteeing that the sufficient condition is satisfied for the optimal control analysis.

The minimized cost function $J_{\min}$ provides another convenient index for determining the optimal region for the placement of the sound sources. In other words, the best region for flutter suppression using acoustics lies in the region where the cost function reaches its minimum. Figure 4a depicts a contour plot of the minimized cost function $J_{\min}$ [Eq. (21)]. This plot is generated by using the data collected from simulations run over a matrix of 151×86 sound source locations, where for each location the optimal control law is designed using the zero-state weighting strategy. The lowest valley of this contour plot appears in the vicinity of the trailing edge, and the local blowup view is shown in Fig. 4b. The distribution of such a minimized cost function along the airfoil surface, however, is illustrated in Fig. 5. From these figures it is concluded that, for an acoustically excited unbounded external flow, the trailing edge is the most effective region for the installation of the acoustic wave generator. Another locally good region is around the midchord of the airfoil.

These results predicted by the optimal control theory basically agree with our previous experiences in discussing the circulatory and noncirculatory parts of the acoustically induced airloads (see Ref. 13), where the midchord and the trailing edge positions carry a special meaning of generating a local and an absolute maximum control force for the harmonically oscillating airfoil motion. Another interesting spot worthy of mentioning is around $x_c \approx 0.83$ on the airfoil surface, namely, the least desirable position for placing the sound source. At this spot the cost function $J_{\min}$ is extremely high (see Fig. 5), the degree of controllability is very low (see Fig. 3), and the flutter suppression effectiveness vanishes (see Ref. 13). In sum, optimal control theory indeed not only yields predictions in compliance with our findings obtained from other independent approaches but also forms a strict mathematical framework for the optimal acoustic flutter control law synthesis.

A comparison study showing the acoustically suppressed system response and the required control effort between using either an optimal state feedback control law or an output feedback control law is performed. The zero-weighting objective function is chosen for designing the optimal state feedback control law, whereas $u = \bar{U}g_\alpha^D y$ is the output feedback control law selected ($\bar{U}=3.15$, $g_\alpha^D=-0.5$). The acoustic excitation position are located at $(0.98, 0^+)$ for both control strategies. The system output responses, control input time histories, and the

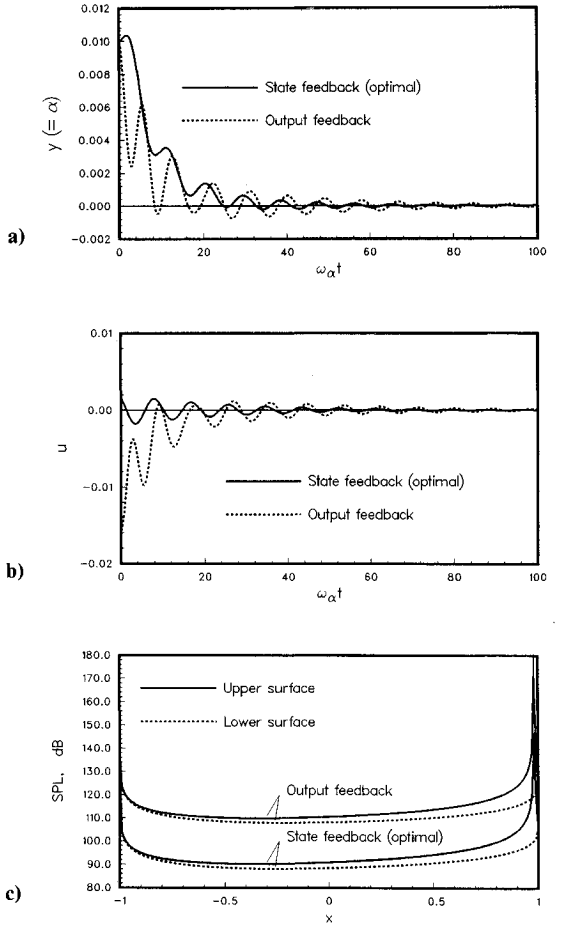

Fig. 6 Comparison of acoustically suppressed system responses using state feedback and output feedback control laws: a) output trajectories, b) control input, and c) sound pressure level distributions ($\bar{U}=3.15$, $x_c=0.98$, $z_c=0^+$).

maximal initial sound pressure level distributions along the upper and lower airfoil surfaces are shown in Figs. 6a–6c, respectively. It is clearly seen that the decaying rates in response are comparable but that the control input for the case using optimal state feedback is much less, in particular at the initial transient stage. If the required control effort is interpreted in terms of sound pressure level, the averaged sound pressure level for the case using the optimal state feedback (about 90 dB) is 20 dB less than that using the output feedback (about 110 dB). This is because in the output feedback control law design only a single system information is detected and fed back, whereas in the optimal full-state feedback design a complete system information has been employed to determine the control input. Hence, the reduction of the required sound pressure level through the use of optimal control law design is illustrated. This control effort minimization will be potentially important for the miniaturization of the sound generator design.

VI. State Observer Design

The state variables defined in the previous control law synthesis usually are not completely accessible from the direct measurements. Nevertheless, we can design a state observer (state estimator) to determine the estimated states from the measured output data. Since the realized dynamic system is completely observable, the information of the states at any time can be obtained from the input and the measured output signals. The *separation principle* assures that the controller and the observer can be designed independently; i.e., the exact states are assumed to be available in designing the full-state feedback control law, which then can be replaced by the estimated states obtained from a parallel design of the state observer.[19] The design of the acoustic flutter controller using SSLQR theory has been previously discussed. In this section the design of the asymptotic state observer is first discussed,

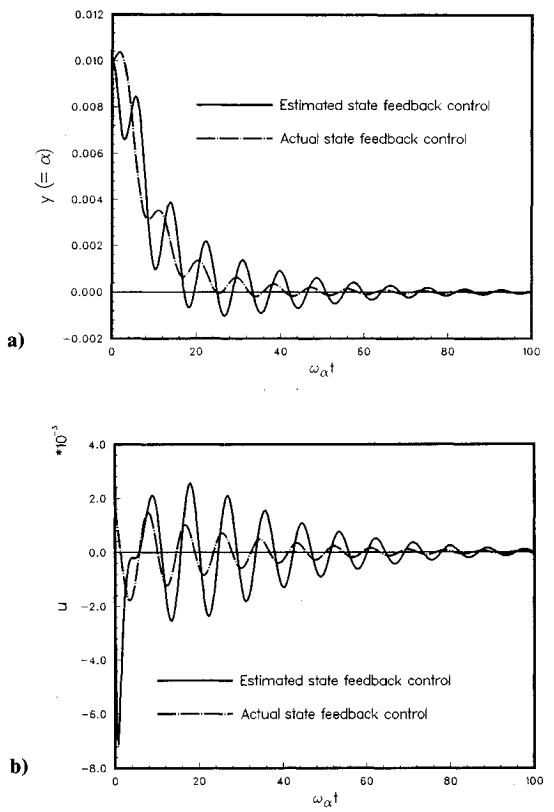

Fig. 7 The output and control input trajectories predicted using SSLQR theory with and without the use of the state estimator: a) output trajectories and b) control inputs [$Q=0$, $R=1$, $y(0)=0.01$, $x_E(0)=0$].

and then a compensator that consists of a controller and a state observer will be illustrated.

The dynamic equation of the asymptotic state observer is given by

$$\frac{d\boldsymbol{x}_E}{d\bar{t}} = \boldsymbol{A}\boldsymbol{x}_E + \boldsymbol{b}u + \boldsymbol{g}_E(y - \boldsymbol{c}\boldsymbol{x}_E) \tag{23}$$

where $\boldsymbol{x}_E$ denotes the estimated state vector and $\boldsymbol{g}_E$ represents the gain vector of the observer that will be determined. Define the error between the actual state vector $\boldsymbol{x}$ and the estimated state $\boldsymbol{x}_E$ as

$$\boldsymbol{e}(\bar{t}) = \boldsymbol{x}(\bar{t}) - \boldsymbol{x}_E(\bar{t}) \tag{24}$$

Then we may have the dynamic equation for the error vector:

$$\frac{d\boldsymbol{e}}{d\bar{t}} = (\boldsymbol{A} - \boldsymbol{g}_E\boldsymbol{c})\boldsymbol{e} \tag{25}$$

Thus, we can choose the observer gain $\boldsymbol{g}_E$ in such a way that all of the eigenvalues of the matrix $(\boldsymbol{A} - \boldsymbol{g}_E\boldsymbol{c})$ have sufficiently large negative real parts. Although a large error might exist between $\boldsymbol{x}(0)$ and $\boldsymbol{x}_E(0)$ initially, the error $\boldsymbol{e}$ would die out quickly as time elapses, and the estimated state $\boldsymbol{x}_E$ will approach the actual state $\boldsymbol{x}$ rapidly, regardless of the initial value of $\boldsymbol{x}_E(0)$. The pole-assignment algorithm[19] is used to design the asymptotic state observer. It is noticed that a fast coalescence of $\boldsymbol{x}_E$ and $\boldsymbol{x}$ requires large negative real parts of the closed-loop eigenvalues of the matrix $(\boldsymbol{A} - \boldsymbol{g}_E\boldsymbol{c})$. This will cause large gains in $\boldsymbol{g}_E$ and generate high peaks in the transient period, making the state estimator either more susceptible to noise or easy to become saturated. As a rule of thumb, the negative real parts of the observer poles can be chosen to be two to six times greater than those of the controller poles. This will result in a fast decay of the estimator errors and let the controller poles dominate the total response.

To solve a control problem with state estimation, the state equation using an estimated state vector as the feedback must be solved simultaneously with the state estimation equation. The overall system dynamics, therefore, reads:

$$\begin{bmatrix} d\boldsymbol{x}/d\bar{t} \\ d\boldsymbol{e}/d\bar{t} \end{bmatrix} = \begin{bmatrix} \boldsymbol{A} + \boldsymbol{b}\boldsymbol{g} & -\boldsymbol{b}\boldsymbol{g} \\ \boldsymbol{0} & \boldsymbol{A} - \boldsymbol{g}_E\boldsymbol{c} \end{bmatrix} \begin{bmatrix} \boldsymbol{x} \\ \boldsymbol{e} \end{bmatrix} \tag{26}$$

It can be shown that the closed-loop eigenvalues of the overall system comprise the eigenvalues of $\boldsymbol{A} + \boldsymbol{b}\boldsymbol{g}$ (the *regulator poles*) and the eigenvalues of $\boldsymbol{A} - \boldsymbol{g}_E\boldsymbol{c}$ (the *observer poles*).

Figures 7a and 7b show the output and input trajectories using the estimated and the actual states, respectively, for feedback (with acoustic excitation located at $x_c = 0.98$, $z_c = 0^+$, and $\bar{U} = 3.15$). The control law is designed from the SSLQR theory with zero-state weighting, and the feedback gains of the observer $\boldsymbol{g}_E$ are chosen such that the real parts of the observer eigenvalues are set at three times the corresponding real parts of the controller eigenvalues. The initial conditions are assumed to be $\alpha(0) = 0.01$, $h(0) = 0$, and $\boldsymbol{x}_E = \boldsymbol{0}$. The discrepancy in the initial states is the source that causes a large control effort initially, but the present state estimator is seen to be able to eliminate the state errors and make the estimator recover the true state asymptotically.

VII. Conclusions

An optimal control law design for the acoustic flutter suppression system is developed. The objective is to propose a complete analysis, including state-space realization, optimal control law synthesis, and observer design that together can be used to minimize the control power required for the generation of the sound waves in suppressing the airfoil fluttering motion. This sound pressure level minimization is of practical importance for the hardware implementation and miniaturization of

the present new flutter suppression technique. The conclusions drawn from the present analysis are:

1) The use of Hankel matrices and the singular value decomposition method makes a systematic approach for irreducibly realizing the present aeroservoelastic system. The dimension of the realized control vector remains unchanged, as compared to the original dynamic system. This property is important for the design and implementation of the present acoustic flutter control problem.

2) The trailing edge is the most efficient region for installing the acoustic wave generator, where the highest degree of controllability exists while the lowest control effort is required. The results predicted by the optimal control theory reconfirm the previous finding discovered in the unsteady aerodynamic and flutter suppression analyses that trailing-edge receptivity holds the key to the present acoustic flutter control technique.

3) An asymptotic observer designed with appropriate closed-loop poles is developed. This observer design can be used to reconstruct the unmeasurable states for the present state-space description of the acoustic flutter control system.

References

[1]Edwards, J. W., Breakwell, J. V., and Bryson, Jr., A. E., "Active Flutter Control Using Generalized Unsteady Aerodynamic Theory," *Journal of Guidance and Control,* Vol. 1, No. 1, 1978, pp. 32–40.

[2]Newsom, J. R., "Control Law Synthesis for Active Flutter Suppression Using Optimal Control Theory," *Journal of Guidance and Control,* Vol. 2, No. 5, 1979, pp. 388–394.

[3]Hwang, C., and Pi, W. S., "Optimal Control Applied to Aircraft Flutter Suppression," *Journal of Guidance, Control, and Dynamics,* Vol. 7, No. 3, 1984, pp. 347–354.

[4]Karpel, M., "Design for Active Flutter Suppression and Gust Alleviation Using State-Space Aeroelastic Modeling," *Journal of Aircraft,* Vol. 19, No. 3, 1982, pp. 221–227.

[5]Karpel, M., "Time Domain Aeroservoelastic Modeling Using Weighted Unsteady Aerodynamic Forces," *Journal of Guidance, Control, and Dynamics,* Vol. 13, No. 1, 1990, pp. 30–37.

[6]Mukhopadhyay, V., Perry, B., III, and Noll, T. E., "Flutter Suppression Control Law Synthesis for the Active Flexible Wing Model," NASA, TM-101584, May 1989.

[7]Liebst, B. S., Garrad, W. L., and Adams, W. M., "Design of an Active Flutter Suppression System," *Journal of Guidance, Control, and Dynamics,* Vol. 9, No. 1, 1986, pp. 64–71.

[8]Nissim, E., "Active Flutter Suppression Using Trailing-Edge and Tab Control Surfaces," *AIAA Journal,* Vol. 14, No. 6, 1976, pp. 757–762.

[9]Nissim, E., "Comparative Study Between Two Different Active Flutter Suppression Systems," *Journal of Aircraft,* Vol. 15, No. 12, 1978, pp. 843–848.

[10]Ffowcs Williams, J. E., "Anti-Sound," *Proceedings of the Royal Society of London,* Series A-395, London, Sept. 1984, pp. 63–88.

[11]Ffowcs Williams, J. E., "The Aeronautical Potential of Anti-Sound," International Council of the Aeronautical Sciences, ICAS-86-01, Amsterdam, The Netherlands, 1986.

[12]Huang, X. Y., "Active Control of Aerofoil Flutter," *AIAA Journal,* Vol. 25, No. 8, 1987, pp. 1126–1132.

[13]Lu, P. J., and Huang, L. J., "Flutter Suppression of Thin Airfoils Using Active Acoustic Excitations," *AIAA Journal,* Vol. 30, No. 12, 1992, pp. 2874–2882.

[14]Theodorsen, T., "General Theory of Aerodynamic Instability and the Mechanism of Flutter," NACA Rept. No. 496, 1935.

[15]Sears, W. R., "Operational Methods in the Theory of Airfoils in Nonuniform Motion," *Journal of the Franklin Institute,* Vol. 230, No. 7, July 1940, pp. 95–111.

[16]Jones, R. T., "The Unsteady Lift of a Wing of Finite Aspect Ratio," NACA Rept. 681, June 1941.

[17]Edwards, J. W., "Unsteady Aerodynamic Modeling for Arbitrary Motions," *AIAA Journal,* Vol. 15, No. 4, 1977, pp. 593–595.

[18]Vepa, R., "On the Padé Approximations to Represent Unsteady Aerodynamic Loads for Arbitrary Small Motions of Wings," AIAA Paper 76-17, Jan. 1976.

[19]Chen, C.-T., *Linear System Theory and Design,* Holt, Rinehart and Winston, New York, 1984.

[20]Kailath, T., *Linear Systems,* Prentice-Hall, Englewood Cliffs, NJ, 1980.

[21]Kalman, R. E., Ho, Y. C., and Narendra, K. S., "Controllability of Linear Dynamic Systems," *Contributions to Differential Equations,* Vol. 1, No. 2, 1963, pp. 189–213.

[22]Friedland, B., "Controllability Index Based on Conditioning Number," *Transactions of ASME, Journal of Dynamic Systems, Measurement, and Control,* Vol. 97G, No. 4, Dec. 1975, pp. 444–445.

[23]Moore, B. C., "Principal Component Analysis in Linear Systems: Controllability, Observability, and Model Reduction," *IEEE Transactions on Automatic Control,* Vol. AC-26, No. 1, 1981, pp. 17–32.

[24]Viswanathan, C. N., Longman, R. W., and Likins, P. W., "A Degree of Controllability Definition: Fundamental Concepts and Application to Modal Systems," *Journal of Guidance, Control, and Dynamics,* Vol. 7, No. 2, 1984, pp. 222–230.

[25]Kwakernaak, H., and Sivan, R., *Linear Optimal Control Systems,* Wiley, New York, 1972.